Comparison of Anisotropic Models to Simulate the Mechanical Response of Facial Skin

Cormac Flynn, Andrew T. Taberner, Sidney Fels and Poul M.F. Nielsen

Abstract Physically-realistic models of the face can contribute to development in several fields including biomedicine, computer animation, and forensics. Face models have benefited from better anatomical representation of the mimetic muscles, and more realistic interactions between soft and bony tissues. These models can also benefit from improved characterisation of the skin layer by having more authentic deformation and wrinkling behaviour. The objective of this work is to compare and evaluate the ability of different constitutive models to simulate the mechanical response of facial skin subjected to a rich set of deformations using a probe. We developed a finite element model to simulate facial skin experiments. Several anisotropic constitutive equations were tested for their suitability to represent facial skin. The finite element model simulated the force-displacement response of facial skin under a rich set of deformations. The variance accounted for between the experimental data and model data ranged from 79% for the Gasser et al. (2006) model to 96% for the Bischoff et al. (2002) model. Estimated pre-stresses ranged from 7 kPa in the lip region to 53 kPa in the central cheek region.

Introduction

Physically realistic biomechanical models of the face can be applied in a wide range of domains, including biomedicine, computer animation and forensics. There has been a continuous improvement in the anatomical accuracy of face models with

C. Flynn (✉)
Centre for Engineering and Industrial Design, Wintec, Hamilton, New Zealand
e-mail: cormac.flynn@wintec.ac.nz

A.T. Taberner · P.M.F. Nielsen
Department of Engineering Science, Auckland Bioengineering Institute,
The University of Auckland, Auckland, New Zealand

S. Fels
Department of Electrical and Computer Engineering, University of British Columbia,
Vancouver, Canada

A. Gefen and D. Weihs (eds.), *Computer Methods in Biomechanics and Biomedical Engineering*, Lecture Notes in Bioengineering,
DOI 10.1007/978-3-319-59764-5_6

better representation of the mimetic muscles, and realistic contact and attachments between soft and bony tissues (Flynn et al. 2015; Wu et al. 2014). Face simulations can also benefit from improved constitutive models of the skin layer. For example, better representation of the mechanical properties of facial skin can lead to improved predictions of deformations as a result of maxillofacial surgical procedures (Zhang et al. 2016).

There is a relative scarcity of facial skin model parameters in the literature. Characterisation studies using suction measurements include Weickenmeier et al. (2015), Luboz et al. (2014), and Ohshima et al. (2011). These approaches do not characterise the anisotropic properties of facial tissues due to the axi-symmetrical nature of the experimental protocol. Ohshima et al. (2011) also used a Reviscometer that characterised the anisotropy of facial skin but this approach assumed skin to have a linear stress–strain response. Few studies attempt to estimate the in vivo pre-stress in facial skin (Flynn et al. 2013). This pre-stress has a significant influence on the behaviour of skin and its inclusion would be an important development in improving the realism of any face model (Swain and Gupta 2015).

This work is a development of the model presented in Flynn et al. (2013). Specifically, the objective is to compare and evaluate several constitutive models and their ability to simulate the mechanical response of facial skin undergoing a rich set of deformations. Material parameter sets will be determined for these constitutive models in addition to estimates of the in vivo pre-stress that is present in facial skin.

Materials and Methods

In Vivo Facial Experiments

The facial skin of several volunteers was subjected to a multi-directional deformation set using a force-sensitive micro-robot (Fig. 1). The experiments are detailed in Flynn et al. (2013). To summarise, we attached a boundary ring to the volunteer's face, centring it on the point of interest. The volunteer rested his head on a support plate (Fig. 2). A 4 mm diameter cylindrical probe was positioned underneath the support plate. A key on the boundary ring matched a hole on the support plate, thus ensuring the orientation of the face with respect to the probe on the micro-robot was known. The probe was attached to the surface of the skin using liquid cyanoacrylate adhesive. We tested several points on the face (Fig. 3). For each location, the probe was moved in 16 different in-plane and out-of-plane directions (Fig. 4). For each direction, three triangular wave cycles of frequency 0.1 Hz were performed to pre-condition the skin. The time, probe displacement, and probe reaction force were recorded via a LabVIEW software interface (National Instruments, Austin, USA).

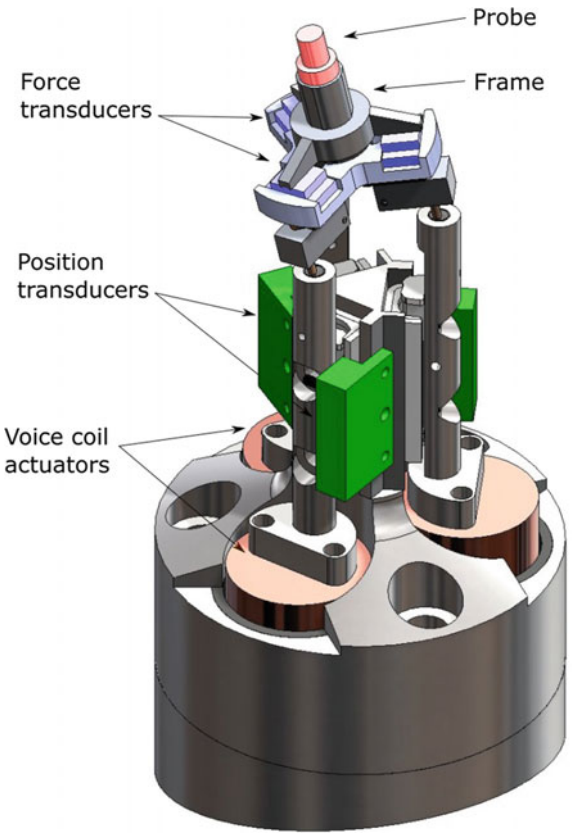

Fig. 1 Force-sensitive micro-robot

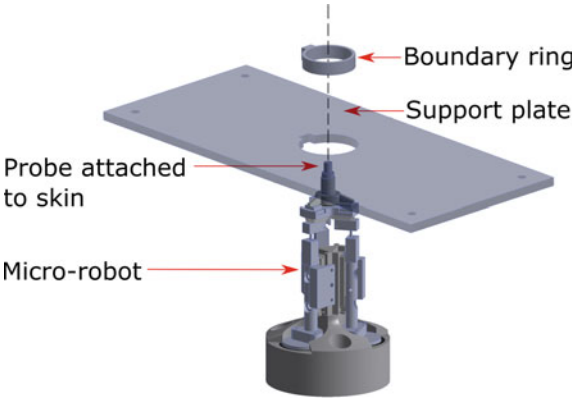

Fig. 2 Experimental setup: the boundary ring is attached to the volunteer's face and centred at one of the locations indicated in Fig. 3

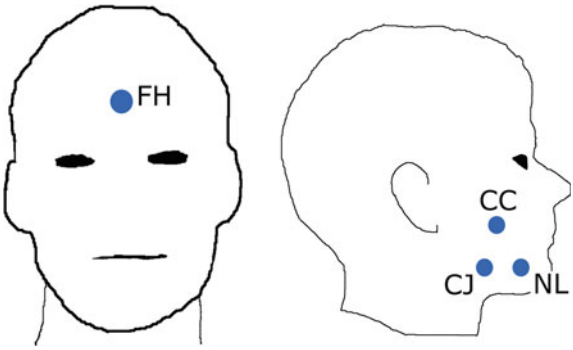

Fig. 3 Locations where the micro-robot probe was attached. *FH* forehead, *CJ* central jaw, *CC* central cheek, *NL* near lip

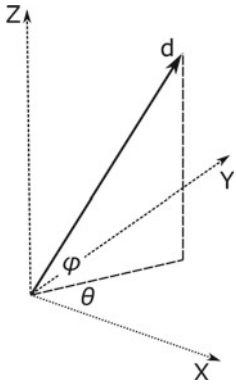

Fig. 4 The probe was displaced in 16 different directions—12 in-plane directions with $\theta = 0°, 30° \ldots 330°$ and $\phi = 0°$, 3 out-of-plane directions with $\theta = 0°, 45°, 90°$ and $\phi = 45°$ and 1 normal direction with $\theta = 0°$ and $\phi = 90°$. $d \approx 1.4$ mm for all directions

Finite Element Model

To simulate the facial skin experiments, we developed a finite element model in FEBio, a package specifically developed to perform nonlinear large deformation analyses in biomechanics (Maas et al. 2012). We modelled the skin as a square domain of side 50 mm (Fig. 5). Two circular partitions of diameter 37.5 and 4 mm were created representing the inside edge of the boundary ring and the outside edge of the probe, respectively. We created the mesh using Gmsh, a three-dimensional finite element mesh generator (Geuzaine and Remacle 2009). It consisted of 2432 quadrilateral shell elements. The thickness of the shell elements was 1.5 mm. A study was undertaken to ensure the mesh density was adequate.

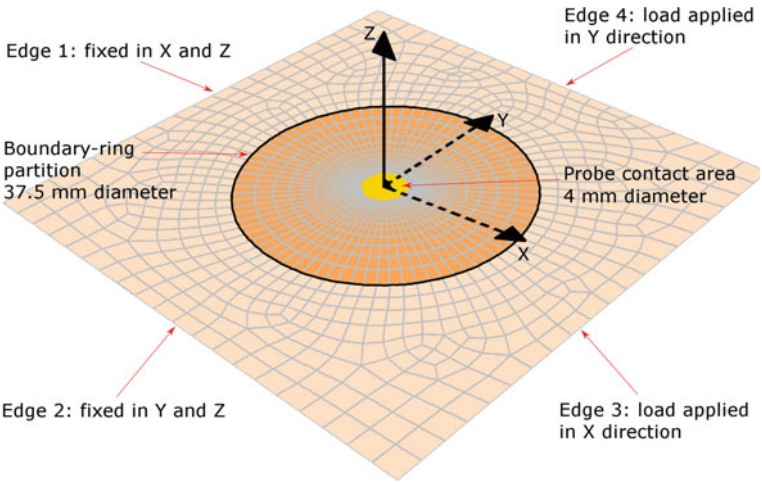

Fig. 5 Finite element model of the in vivo experiments

In an initial static analysis step, we applied a pre-stress (σ_x, σ_y) to the skin. Edge 1 was fixed in the X direction and edge 2 was fixed in the Y direction (Fig. 5). All four edges of the square were fixed in the Z direction. A load in the Y direction was applied to each node along edge 3 and a load in the X direction was applied to each node along edge 4. The loads were linearly increased from zero to the full load in 5 s.

In the second static analysis step, all the nodes outside the boundary-ring partition were fixed in all degrees of freedom. These conditions reflect the assumption that any skin outside the boundary ring did not move in the experiments. The nodes inside the probe area were displaced according to the in vivo experimental protocol. The total of the nodal reaction forces inside the probe region was calculated for the full cycle.

Constitutive Models

We investigated the suitability of three constitutive models to represent the mechanical behaviour of skin.

The orthotropic Bischoff et al. (2002) model is based on an assembly of eight fibres arranged within a unit cell. The orthotropic response is determined by the relative length of the cell edges a, b and c. This constitutive equation was implemented into FEBio using the user material plug-in facility. The strain energy function is

$$W_{\text{Bischoff}} = \frac{nk\theta}{4}\left(P^2\sum_{i=1}^{4}\left[\frac{\rho^{(i)}}{P^2}\beta_\rho^{(i)} + \ln\frac{\beta_\rho^{(i)}}{\sinh\beta_\rho^{(i)}}\right] - \frac{\beta_P}{P}\ln\left[\bar{\lambda}_{\mathbf{a}}^{a^2}\bar{\lambda}_{\mathbf{b}}^{b^2}\bar{\lambda}_{\mathbf{c}}^{c^2}\right]\right) + U(J) \quad (1)$$

where n is the number of fibres per unit volume, $k = 1.38 \times 10^{-23}\,\text{JK}^{-1}$ is Boltzman's constant, and θ is the absolute temperature.

$\bar{\lambda}_{\mathbf{a}} = \sqrt{\mathbf{a}^T\bar{\mathbf{C}}\mathbf{a}}$, $\bar{\lambda}_{\mathbf{b}} = \sqrt{\mathbf{b}^T\bar{\mathbf{C}}\mathbf{b}}$, $\bar{\lambda}_{\mathbf{c}} = \sqrt{\mathbf{c}^T\bar{\mathbf{C}}\mathbf{c}}$ are the principal fibre stretches along the principal material axes of the unit cell, $(\mathbf{a}, \mathbf{b}, \mathbf{c})$. $\bar{\mathbf{C}}$ is the deviatoric right Cauchy tensor.

$P = \frac{1}{2}\sqrt{a^2 + b^2 + c^2}$ is the undeformed length of a fibre in the cell, while $\rho^{(i)}$ is the deformed length of the ith fibre. $\beta_\rho^{(i)} = \mathcal{L}^{-1}\left(\frac{\rho^{(i)}}{N}\right)$, with $\mathcal{L}(x) = \coth x - \frac{1}{x}$ being the Langevin function.

The volumetric component of the strain energy function is

$$U(J) = \frac{B}{2}(\ln J)^2 \quad (2)$$

where $B = 1$ MPa is the bulk modulus and $J = det\mathbf{F}$ is the volume ratio. $\mathbf{F}$ is the deformation gradient.

The second model tested was a frame invariant version of the Fung constitutive equation (Ateshian and Costa 2009).

$$W_{\text{Fung}} = \frac{c}{2}\left(\mathrm{e}^{Q} - 1\right) + U(J) \quad (3)$$

$$Q = c^{-1}\sum_{a=1}^{3}\left[2\mu_a\mathbf{a}_a^0 \otimes \mathbf{a}_a^0 : \bar{\mathbf{E}}^2 + \sum_{b=1}^{3}\lambda_{ab}\left(\mathbf{a}_a^0 \otimes \mathbf{a}_a^0 : \bar{\mathbf{E}}\right)\left(\mathbf{a}_b^0 \otimes \mathbf{a}_b^0 : \bar{\mathbf{E}}\right)\right] \quad (4)$$

where c is a parameter representing the stiffness, and λ_{ab}, μ_a are Lamé parameters. All parameters have units of stress. $\bar{\mathbf{E}} = \frac{1}{2}(\bar{\mathbf{F}}^T\bar{\mathbf{F}} - \mathbf{I})$ is the deviatoric Green–Lagrange strain tensor. $\mathbf{a}_a^0$ defines an initial direction of a material axis a. For the purposes of simplifying the parameter optimisation procedure, $\lambda_{11} = \lambda_{12} = \lambda_{23} = \lambda_{31}$, $\lambda_{22} = \lambda_{33}$, and $\mu_2 = \mu_3$.

The third constitutive model tested was an anisotropic model proposed by Gasser et al. (2006).

$$W_{\text{Gasser}} = \frac{\mu}{2}(\bar{I}_1 - 1) + \frac{k_1}{k_2}\left\{\mathrm{e}^{k_2[\tilde{I}_n(\theta)-1]^2} - 1\right\} + U(J) \quad (5)$$

where μ, k_1 control the stiffness of the skin at small strains and k_2 is a dimensionless parameter that controls the stiffness at large strains. $\tilde{I}_n(\theta) = \mathbf{N}\bar{\mathbf{C}}\mathbf{N}$ is the fibre stretch

squared of the nth family of fibres orientated in the direction $\mathbf{N}$ in the reference configuration.

For all the strain energy functions described, we used a quasi-linear viscoelastic model to characterise the time-dependent properties of skin (Fung 1993).

$$\mathbf{T}(t) = \mathbf{T}_e(t) + \int_0^t \mathbf{T}_e(t-\tau)\frac{\partial g_R(\tau)}{\partial \tau}\,\mathrm{d}\tau, \tag{6}$$

where $\mathbf{T}(t)$ is the total Cauchy stress at time t, $\mathbf{T}_e = \frac{1}{J}\mathbf{F}\frac{\partial W}{\partial E}\mathbf{F}^T$ is the elastic Cauchy stress, and $g_r(t)$ is a Prony series relaxation function.

$$g_R(t) = 1 - \bar{g}_1^P\left(1 - \mathrm{e}^{-t/\tau_1^G}\right) \tag{7}$$

where $\bar{g}_1^P = 0.4$ is a viscoelastic parameter and $\tau_1^G = 0.8\,s$ is the relaxation time.

Parameter Identification Framework

Using a framework developed in MATLAB 2016a (The MathWorks, Inc., Natick, MA, USA), we identified the material parameters and pre-stress field that best fit the probe reaction forces from the model to the measured probe reaction forces from the experiments. Optimised parameter sets using each constitutive model were determined.

Similar to Flynn et al. (2013), the following objective function was minimised in a least-squares sense using the *lsqnonlin* function in Matlab:

$$F(\mathbf{x}) = \sum_{i=1}^{16}\sum_{j=1}^{N_i}\left\{\left(\frac{R_{X_j}^{\mathrm{model}}(\mathbf{x}) - R_{X_j}^{\mathrm{exp}}}{\max\left(R_{X_j}^{\mathrm{exp}}\right)}\right)^2 + \left(\frac{R_{Y_j}^{\mathrm{model}}(\mathbf{x}) - R_{Y_j}^{\mathrm{exp}}}{\max\left(R_{Y_j}^{\mathrm{exp}}\right)}\right)^2 + \left(\frac{R_{Z_j}^{\mathrm{model}}(\mathbf{x}) - R_{Z_j}^{\mathrm{exp}}}{\max\left(R_{Z_j}^{\mathrm{exp}}\right)}\right)^2\right\} \tag{8}$$

where $\mathbf{x}$ is the model parameter set, and N_i is the number of data points recorded for the ith probe direction (16 directions in total). $R_{X_j}^{\mathrm{model}}(\mathbf{x})$, $R_{Y_j}^{\mathrm{model}}(\mathbf{x})$, and $R_{Z_j}^{\mathrm{model}}(\mathbf{x})$ are the model probe reaction forces in the X, Y, and Z directions at the jth data point. $R_{X_j}^{\mathrm{exp}}$, $R_{Y_j}^{\mathrm{exp}}$, $R_{Z_j}^{\mathrm{exp}}$ are the experiment probe reaction forces in the X, Y and Z directions at the jth data point.

The procedure of the MATLAB script for the optimisation was as follows. Starting with initial material parameters and a pre-stress field, a simplified mesh with no partitions was subjected to the boundary and load conditions specified in the first static step described in the Finite element model section. This step determined the stretch of the model in the X and Y directions. Using the stretch information, a Gmsh script created the full finite element mesh with partitions described

in the Finite element model section. The geometries of the boundary and probe partitions were such that when the pre-stress was applied to this mesh in the initial step, both these partitions were circular and their diameters corresponded to those of the experiment. The second step with the nodes in the probe region being displaced was then executed.

When all analyses were complete, the objective function in Eq. (8) was calculated. The material parameters and pre-stresses were then adjusted by the *lsqnonlin* function. Updated FEBio and Gmsh input files were created and the analyses executed again. This iterative process continued until the objective function reached a local minimum.

We identified parameter sets that best fit the model data to in vivo data for different points of the face. For each optimised set, the variance accounted for (*VAF*) was calculated.

$$\mathrm{VAF} = 1 - \frac{F(\mathbf{x})}{\sum_{i=1}^{16}\sum_{j=1}^{N_i}\left\{\left(\frac{R_{X_j}^{\exp}}{\max\left(R_{X_j}^{\exp}\right)}\right)^2 + \left(\frac{R_{Y_j}^{\exp}}{\max\left(R_{Y_j}^{\exp}\right)}\right)^2 + \left(\frac{R_{Z_j}^{\exp}}{\max\left(R_{Z_j}^{\exp}\right)}\right)^2\right\}} \tag{9}$$

The results were compared with the results using the Ogden (1972) model reported in Flynn et al. (2013).

Results

Through the nonlinear optimisation procedure, we identified the material parameters and pre-stresses that best fit several constitutive models to in vivo experimental data (Tables 1, 2, 3 and 4). The lowest *VAF* was 79% for the Gasser et al. (2006) model when simulating the skin deformation in the forehead region Table 1. The

Table 1 Forehead region: identified material parameters, in vivo pre-stress field, and variance accounted for (*VAF*)

Model	Model parameters	(σ_x, σ_y) (kPa)	*VAF* (%)
Bischoff et al. (2002)	$n = 6.632 \times 10^{11}\,\mathrm{mm}^{-3}$; $(a, b, c) = (0.8529, 1.272, 1.386)$	(24.52, 22.73)	94
Ateshian and Costa (2009)	$c = 0.3118$ kPa; $\lambda_{11} = 0.9982$ kPa; $\lambda_{22} = 1.005$ kPa; $\mu_1 = 7.169$ kPa; $\mu_2 = 7.142$ kPa	(7.336, 3.351)	94
Gasser et al. (2006)	$\mu = 14.08$ kPa; $k_1 = 11.01$ kPa; $k_2 = 0.09188$; $\theta = 30.82^o$	(25.65, 17.67)	79
Ogden (1972)	$\mu_1 = 53.95$ kPa; $\mu_2 = 0.3012$ Pa; $\alpha_1 = 1.868$; $\alpha_2 = 69.00$	(34.12, 26.72)	94

The Ogden (1972) parameters are from Flynn et al. (2013)

Table 2 Near lip region: Identified material parameters, in vivo pre-stress field, and variance accounted for (*VAF*)

Model	Model parameters	(σ_x, σ_y) (kPa)	VAF (%)
Bischoff et al. (2002)	$n = 5.690 \times 10^{11}\text{mm}^{-3}$; $(a, b, c) = (0.6952, 1.276, 1.529)$	(9.088, 7.904)	94
Ateshian and Costa (2009)	$c = 0.3291$ kPa; $\lambda_{11} = 1.0$ kPa; $\lambda_{22} = 6.387$ kPa; $\mu_1 = 4.556$ kPa; $\mu_2 = 2.352$ kPa	(9.121, 7.342)	91
Ogden (1972)	$\mu_1 = 41.29$ kPa; $\mu_2 = 0.16$ Pa; $\alpha_1 = 1.658$; $\alpha_2 = 54.964$	(24.2, 15.9)	93

The Ogden (1972) parameters are from Flynn et al. (2013)

Table 3 Central cheek region: identified material parameters, in vivo pre-stress field, and variance accounted for (*VAF*)

Model	Model parameters	(σ_x, σ_y) (kPa)	*VAF* (%)
Bischoff et al. (2002)	$n = 1.246 \times 10^{12}\text{mm}^{-3}$; $(a, b, c) = (0.7880, 1.246, 1.446)$	(52.52, 45.98)	92
Ateshian and Costa (2009)	$c = 0.4421$ kPa; $\lambda_{11} = 1.0$ kPa; $\lambda_{22} = 1.0$ kPa; $\mu_1 = 6.121$ kPa; $\mu_2 = 4.353$ kPa	(9.518, 4.970)	93
Ogden (1972)	$\mu_1 = 58.27$ kPa; $\mu_2 = 0.14$ Pa; $\alpha_1 = 2.334$; $\alpha_2 = 33.081$	(89.4, 71.8)	93

The Ogden (1972) parameters are from Flynn et al. (2013)

Table 4 Central jaw region: identified material parameters, in vivo pre-stress field, and variance accounted for (*VAF*)

Model	Model parameters	(σ_x, σ_y) (kPa)	VAF (%)
Bischoff et al. (2002)	$n = 8.922 \times 10^{11}\text{mm}^{-3}$; $(a, b, c) = (0.8406, 1.224, 1.413)$	(36.88, 31.66)	96
Ateshian and Costa (2009)	$c = 0.5010$ kPa; $\lambda_{11} = 1.000$ kPa; $\lambda_{22} = 1.000$ kPa; $\mu_1 = 3.322$ kPa; $\mu_2 = 5.919$ kPa	(20.33, 15.84)	95
Ogden (1972)	$\mu_1 = 57.73$ kPa; $\mu_2 = 0.42$ Pa; $\alpha_1 = 2.265$; $\alpha_2 = 34.689$	(81.3, 75.4)	96

The Ogden (1972) parameters are from Flynn et al. (2013)

highest *VAF* was 96% for both the Bischoff et al. (2002) and Ogden (1972) models when simulating deformations in the central jaw region (Table 4).

The Bischoff et al. (2002) model simulated the nonlinear, anisotropic, and viscoelastic response of forehead skin observed in the experiments (Fig. 6). The results of the model for the other facial regions were similar. The Ateshian and Costa (2009)

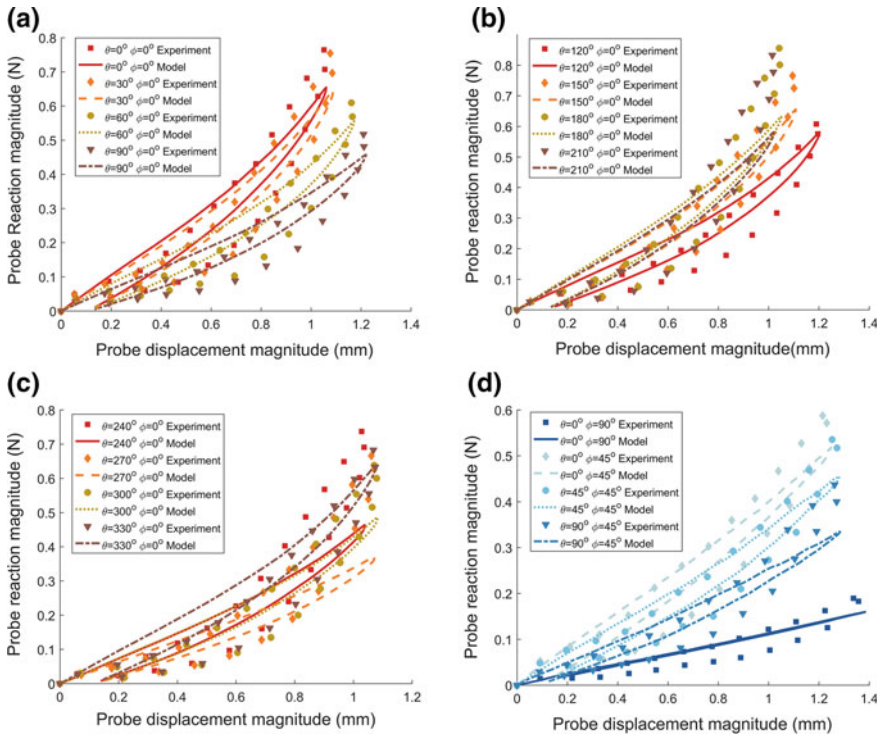

Fig. 6 Experiment and Bischoff et al. (2002) model probe reaction–displacement response for forehead region. **a**–**c** in-plane response; **d** out-of-plane response. *VAF* for Bischoff et al. (2002) was 94%. See Table 1 for model parameters and pre-stresses

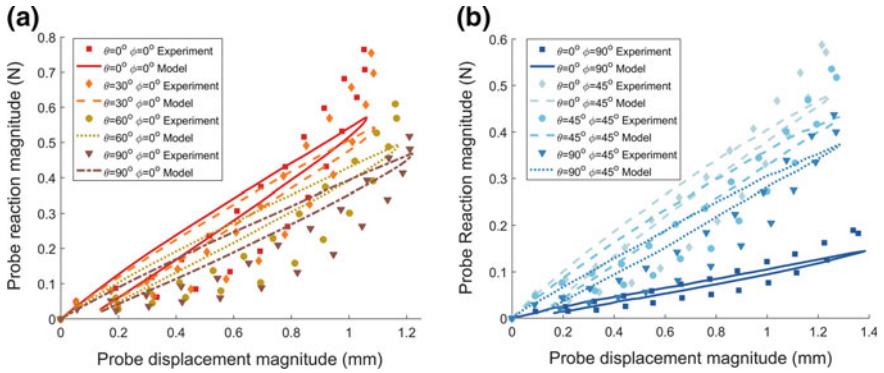

Fig. 7 Experiment and Gasser et al. (2006) model probe reaction–displacement response for forehead region. **a** sample of in-plane response; **b** out-of-plane response. *VAF* for Gasser et al. (2006) was 79%. See Table 1 for model parameters and pre-stresses

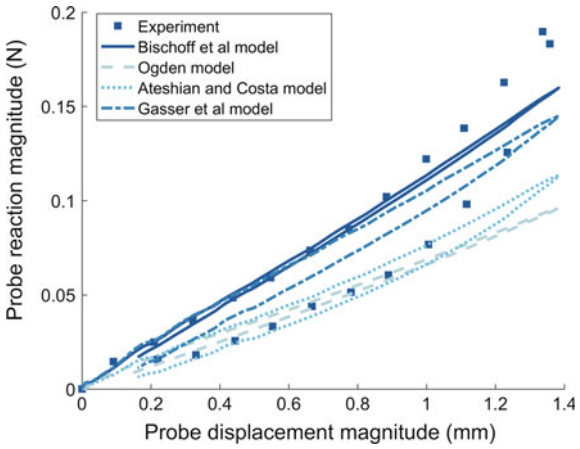

Fig. 8 Comparison of the forehead region normal response ($\theta = 0°, \phi = 90°$) of the models to the experimental measurement

model exhibited similar behaviour to the Bischoff et al. (2002) model (results not shown). The *VAF*s for both models in all regions were similar.

The Gasser et al. (2006) model did not simulate the nonlinear response of the forehead skin as well as the other models (Fig. 7).

The constitutive models simulated the normal deformation of the forehead region with varying degrees of accuracy (Fig. 8). The peak probe reaction force of the Ateshian and Costa (2009) model was approximately 50% of the measured force. The Bischoff et al. (2002) model simulated a maximum reaction force that was approximately 85% of the measured normal response.

Discussion

The force response of several facial regions undergoing a rich set of deformations has been simulated by a finite element model. Three anisotropic constitutive equations were tested and the *VAF* between the model and the experimental results ranged from 79% to 96%.

For each constitutive equation, the material parameter values varied considerably according to facial region. This demonstrates the need to measure the response at many points to develop a realistic facial model.

The *VAF*s using the Bischoff et al. (2002), Ateshian and Costa (2009) and Ogden (1972) models were very similar and differed by no more than a few per cent at each facial location. In contrast, the *VAF* for the Gasser et al. (2006) model was poor compared to the other models and its force–displacement response was too linear. Using anisotropic constitutive models did not yield better results than using the isotropic Ogden (1972) model. However, if knowledge of the collagen fibre distributions were obtained from appropriate imaging, this information could be used by the anisotropic models and could yield improved results.

In general, the force response of the model at small probe displacements was too high compared to the experimental force response. This contrasts with the Ogden (1972) model results reported in Flynn et al. (2013). In that study, there was better agreement between model and experiment at lower displacements than at higher displacements.

The estimated pre-stress in a region varied according to the constitutive model used. For example, in the forehead region, using the Ateshian and Costa (2009) model resulted in a pre-stress in the X direction of 7.336 kPa and 3.351 kPa in the Y direction Table 1. This was a lower pre-stress than estimated by the other models. When comparing the normal force–displacement responses, the Ateshian and Costa (2009) model had the poorest agreement with the experimental data (Fig. 8). Flynn et al. (2011) demonstrated that the calculated normal response of skin is more dependent on the pre-stress than the material parameters. This idea has been explored in calculating the wall stress in cerebral aneurysms (Lu et al. 2008). The estimated pre-stress using the Bischoff et al. (2002) model (24.52 kPa, 22.73 kPa) was similar to the pre-stress estimated using the Gasser et al. (2006) model (25.65 kPa, 17.67 kPa). Their respective normal force–displacement responses were also similar (Fig. 8). However, the estimated pre-stress using the Ogden (1972) model was the highest (34.12 kPa, 26.72 kPa) but the corresponding normal response did not match the experimental data. Further investigation is needed to determine the effect of the constitutive model on the estimated pre-stress and normal response.

There was some asymmetry in the measured force–displacement response. The simplistic nature of the model does not allow this asymmetry to be simulated. Improvements should be observed if the sub-dermal layers and their attachments are represented.

References

Ateshian GA, Costa KD (2009) A frame-invariant formulation of Fung elasticity. J Biomech 42 (6):781–785

Bischoff JE, Arruda EA, Grosh K (2002) A microstructurally based orthotropic hyperelastic constitutive law. J Appl Mech Trans ASME 69(5):570–579

Flynn C, Taberner A, Nielsen P (2011) Modeling the mechanical response of in vivo human skin under a rich set of deformations. Ann Biomed Eng 39(7):1935–1946

Flynn C, Taberner AJ, Nielsen PMF, Fels S (2013) Simulating the threedimensional deformation of in vivo facial skin. J Mech Behav Biomed Mater 28:484–494

Flynn C, Stavness I, Lloyd J, Fels S (2015) A finite element model of the face including an orthotropic skin model under in vivo tension. Comput Methods Biomech Biomed Eng 18 (6):571582

Fung YC (1993) Biomechanics: mechanical properties of living tissues. Springer, New York

Gasser TC, Ogden RW, Holzapfel GA (2006) Hyperelastic modelling of arterial layers with distributed collagen fibre orientations. J R Soc Interface 3(6):15–35

Geuzaine C, Remacle J-F (2009) Gmsh: A 3-D finite element mesh generator with built-in pre-and post-processing facilities. Int J Numer Methods Eng 79(11):1309–1331

Lu J, Zhou X, Raghavan ML (2008) Inverse method of stress analysis for cerebral aneurysms. Biomech Model Mechanobiol 7(6):477–486

Luboz V, Promayon E, Payan Y (2014) Linear elastic properties of the facial soft tissues using an aspiration device: towards patient specific characterization. Ann Biomed Eng 42(11):2369–2378

Maas SA, Ellis BJ, Ateshian GA, Weiss JA (2012) FEBio: finite elements for biomechanics. J Biomech Eng 134(1):011005

Ogden RW (1972) Large deformation isotropic elasticity—on the correlation of theory and experiment for incompressible rubberlike solids. Proc R Soc Lond A Math Phys Sci 326 (1567):565–584

Ohshima H, Tada A, Kanamaru A, Akamatsu H, Sakai Y, Itoh M, Kanto H (2011) Relevance of the directionality of skin elasticity to aging and sagging of the face. Skin Res Technol 17(1):101–107

Swain D, Gupta A (2015) Interfacial growth during closure of a cutaneous wound: stress generation and wrinkle formation. Soft Matter 11(32):6499–6508

Weickenmeier J, Jabareen M, Mazza E (2015) Suction based mechanical characterization of superficial facial soft tissues. J Biomech 48(16):4279–4286

Wu T-F, Hung A, Mithraratne K (2014) Generating facial expressions using an anatomically accurate biomechanical model. IEEE Trans Vis Comput Graph 20(11):1519–1529

Zhang X, Tang Z, Liebschner MA, Kim D, Shen S, Chang C-M, Yuan P, Zhang G, Gateno J, Zhou X et al (2016) An eFace-template method for efficiently generating patient-specific anatomically-detailed facial soft tissue FE models for craniomaxillofacial surgery simulation. Ann Biomed Eng 44(5):1656–1671